THE JOURNAL OF BIOLOGICAL CHEMISTRY VOL. 283, NO. 50, pp. 35154–35163, December 12, 2008

Structural Basis of the Migfilin-Filamin Interaction and Competition with Integrin β Tails*[S]

Received for publication, April 3, 2008, and in revised form, September 9, 2008 Published, JBC Papers in Press, September 30, 2008, DOI 10.1074/jbc.M802592200

Yatish Lad[‡1], Pengju Jiang[§1,2], Salla Ruskamo[¶1,3], David S. Harburger[‡4], Jari Ylänne[¶], Iain D. Campbell[§], and David A. Calderwood[‡5]

From the [‡]Department of Pharmacology and Interdepartmental Program in Vascular Biology and Transplantation, Yale University School of Medicine, New Haven, Connecticut 06520, the [§]Department of Biochemistry, University of Oxford, Oxford OX1 3QU, United Kingdom, and the [¶]Department of Biological and Environmental Science, University of Jyväskylä, FIN-40014 Jyväskylä, Finland

A link between sites of cell adhesion and the cytoskeleton is essential for regulation of cell shape, motility, and signaling. Migfilin is a recently identified adaptor protein that localizes at cell-cell and cell-extracellular matrix adhesion sites, where it is thought to provide a link to the cytoskeleton by interacting with the actin cross-linking protein filamin. Here we have used x-ray crystallography, NMR spectroscopy, and protein-protein interaction studies to investigate the molecular basis of migfilin binding to filamin. We report that the N-terminal portion of migfilin can bind all three human filamins (FLNa, -b, or -c) and that there are multiple migfilin-binding sites in FLNa. Human filamins are composed of an N-terminal actin-binding domain followed by 24 immunoglobulin-like (IgFLN) domains and we find that migfilin binds preferentially to IgFLNa21 and more weakly to IgFLNa19 and -22. The filamin-binding site in migfilin is localized between Pro[5] and Pro[19] and binds to the CD face of the IgFLNa21 β-sandwich. This interaction is similar to the previously characterized β7 integrin-IgFLNa21 interaction and migfilin and integrin β tails can compete with one another for binding to IgFLNa21. This suggests that competition between filamin ligands for common binding sites on IgFLN domains may provide a general means of modulating filamin interactions and signaling. In this specific case, displacement of integrin tails from filamin by migfilin may provide a mechanism for switching between different integrin-cytoskeleton linkages.

Functional connections between transmembrane adhesion receptors and the intracellular cytoskeleton permit transmission of biochemical signals and mechanical force across the plasma membrane and are essential to the development and functioning of multicellular animals (1). In many cases connections are formed at specialized sites involving assemblies of many adhesion molecules and cytoskeletal and signaling adaptors (2). Although many components of these adhesion complexes have now been identified, a complete understanding of how adhesion complexes function will require detailed information on individual components and how they interact or compete with other elements of this complex machinery. Here we characterize the interaction of a recently identified adaptor protein, migfilin, with the actin-binding protein filamin and examine how this influences interactions of filamin with integrin adhesion receptors.

Migfilin, also termed filamin-binding LIM protein-1, is a LIM domain protein that localizes to both cell-extracellular matrix and cell-cell contact sites, where it is thought to provide a link between the actin cytoskeleton and integrin-extracellular matrix contact sites and cadherin-catenin cell-cell junctions, respectively (3–5). In this way, migfilin can modulate cell shape, migration, and cadherin-mediated cell-cell contacts. Increased migfilin expression is observed in human leiomyosarcoma and expression levels correlate with tumor grade although the molecular basis for this observation remains to be determined (6). Approximately 50 kDa in size, migfilin is composed of three C-terminal LIM domains, a central proline-rich region, and an N-terminal portion, which lacks any identifiable structural domains or sequence motifs. Alternative splicing can result in removal of the final LIM domain or the proline-rich region (5). The LIM domains mediate binding to kindlin-2 (Mig-2) and are required for localization to focal adhesions (3). The central proline-rich domain has recently been shown to bind to vasodilator-stimulated phosphoprotein, an interaction observed to be important for migfilin modulation of cell migration (7). The N-terminal region binds to filamins (3, 4) and this interaction is thought to provide a link to the actin cytoskeleton.

Vertebrates have three homologous genes that encode filamin A, B, and C: of these, filamin A (FLNa)[6] is the most abundant and widely expressed (8, 9). These filamins are non-covalent dimers of two 280-kDa subunits composed of an

* This work was supported, in whole or in part, by National Institutes of Health Grant GM068600 (to D. A. C.). This work was also supported by Academy of Finland Grant 114713 (to J. Y.). The costs of publication of this article were defrayed in part by the payment of page charges. This article must therefore be hereby marked "*advertisement*" in accordance with 18 U.S.C. Section 1734 solely to indicate this fact.

The atomic coordinates and structure factors (code 2W0P) have been deposited in the Protein Data Bank, Research Collaboratory for Structural Bioinformatics, Rutgers University, New Brunswick, NJ (http://www.rcsb.org/).

[S] The on-line version of this article (available at http://www.jbc.org) contains supplemental Fig. S1.

[1] These authors contributed equally to this work.

[2] Supported by Biotechnology and Biological Sciences Research Council Grant BB/F006845/1.

[3] Supported by the Finnish Graduate School in Informational and Structural Biology.

[4] Supported by a National Science Foundation Graduate Research Fellowship Award.

[5] To whom correspondence should be addressed: Dept. of Pharmacology, Yale University School of Medicine, 333 Cedar St., P.O. Box 208066, New Haven, CT 06520-8066. Tel.: 203-737-2311; Fax: 203-785-7670; E-mail: david.calderwood@yale.edu.

[6] The abbreviations used are: FLNa, filamin A; ABD, actin-binding domain; GST, glutathione *S*-transferase.

N-terminal actin-binding domain (ABD) followed by 24 immunoglobulin-like domains (IgFLN1–24) with IgFLN24 mediating dimerization (10, 11). A flexible hinge region separates IgFLN1–15 (rod 1), which contains a secondary actin-binding site and IgFLN16–24 (rod 2) allowing filamin to stabilize high angle actin fiber cross-links (12). In addition to their role as actin cross-linking proteins, filamins, mostly through their C-terminal domains, IgFLN16–24, bind an array of cytosolic signaling and adaptor proteins and transmembrane receptors (8, 13, 14), suggesting that filamins play complex and diverse roles within the cell.

We have previously identified IgFLNa21 as the major binding site in FLNa for integrin adhesion receptors and the structure of IgFLNa21 in complex with a β7 integrin peptide showed that IgFLNa21 forms a β-sandwich composed of two β-sheets (15). The CD face of the IgFLNa21 β-sandwich is the major interaction site for the β7 integrin peptide. NMR, mutagenesis, and structures of other IgFLN-ligand interactions suggested that the CD face of IgFLN domains represents a common interface for filamin-ligand binding (15). Yeast two-hybrid studies and GST-FLNc pull-down assays from cell lysates have mapped migfilin binding to IgFLNc21 and IgFLNa19–24 (3). This overlap in the binding specificity of IgFLN21 for migfilin and β-integrin tails raises the following intriguing questions: 1) does migfilin bind the CD face of IgFLN21 in a manner analogous to the interaction between IgFLNa21 and β7 integrin peptide and 2) do migfilin and integrins compete for binding to the same IgFLNa21 protein? More recently a migfilin splice variant (FBLP-1) with an identical N-terminal region to migfilin was shown to interact with IgFLNb10–13, suggesting a potential secondary migfilin binding site within filamins (4). Using biochemical and NMR structure-based analyses we find that FLNa contains multiple migfilin-binding sites; that the N terminus of migfilin is relatively unstructured and, upon binding to IgFLNa21, perturbs residues in the CD face in a similar way to peptides derived from β7 integrin. X-ray crystallography and analysis of mutant proteins reveals the molecular basis of IgFLNa21-migfilin interactions. The interaction between migfilin and IgFLNa21 is capable of competing with integrins because it is of higher affinity. Displacement of integrin tails by migfilin could provide a mechanism for switching from one type of integrin/cytoskeleton linkage to another, perhaps involving kindlin-2 in some cell types.

EXPERIMENTAL PROCEDURES

Antibodies and DNAs—Monoclonal antibodies, activating anti-β1 integrin 9EG7 (BD Biosciences), anti-mouse CD29 (Biolegend) and anti-His (Novagen), and polyclonal anti-GST (Chemicon), anti-GFP (Rockland) were obtained commercially. The anti-FLNa polyclonal antibody has been described previously (15). cDNAs encoding migfilin amino acids 1–85 or 86–373 were generated by polymerase chain reaction (PCR) and subcloned into pET28A (Novagen) or pEGFP (BD Biosciences) (AY180161). FLNa-GFP has been described previously (NM_001456) (16), FLNa-(1–1761)-GFP (ABD + rod 1) and FLNa-(1762–2647)-GFP (Ig16–24; rod 2) were generated by PCR, FLNb-GFP was provided by A. Sonnenberg (Netherlands Cancer Centre, Netherlands) (17). FLNc-GFP was a gift from D. O. Fürst and P. F. M. van der Ven (University of Bonn, Germany), GST-IgFLNa19, -20, -21, -22, and -23, and IgFLNa21 AA/ST, AA/DK, I/C, and I/M have been described previously (15). Point mutations were introduced with the QuikChange site-directed mutagenesis kit (Stratagene) and confirmed by DNA sequencing.

Pull-down Assays with Migfilin—Recombinant migfilin proteins were produced as described for integrin tail proteins and GST-filamin fragments were produced and purified as described previously (15, 18). Pull-down assays were performed using recombinant migfilin bound to His-bind resin (Novagen) as described previously (18); bound proteins were fractionated by SDS-PAGE and analyzed by Western blotting or protein staining. Migfilin peptide (amino acids 5–19) and control (reverse sequence) were obtained from Tufts University Core Facility, Boston, MA. To estimate apparent affinity constants the binding of increasing amounts of purified GST-IgFLNa21 proteins to migfilin tails was quantified by densitometry; data were plotted as percent maximal binding *versus* input concentration and fitted to a one site binding model ($Y = B_{max} \times X/(K_d + X)$) using GraphPad Prism version 4 for Windows (GraphPad Software).

Immunofluorescence—NIH3T3 cells were transfected with the indicated cDNAs using Lipofectamine (Invitrogen) and 24 h later were detached, allowed to re-adhere, and spread on fibronectin-coated coverslips. After 4 h of plating, cells were fixed, permeabilized, and stained with anti-filamin or Alexa Fluor 568-phalloidin (Invitrogen) as described previously (15, 19).

NMR—The uniformly ^{15}N-labeled samples, IgFLNa21 (residue 2236–2329) and IgFLNa19 (residue 2045–2141) were prepared and assigned using the strategy described in our earlier publications (15, 16). The migfilin-(1–85) was subcloned into a pET-28a vector and produced in non-labeled and ^{15}N-labeled forms following the manufacturer's protocol (Novagen), whereas the synthetic migfilin-derived peptides (all N-terminal acetylated and C-terminal amidated) were purchased from EZbiolab.

All NMR samples were buffered in 50 mM sodium phosphate and 100 mM sodium chloride with 10% D_2O added at pH 6.10 and 25 °C. The HSQC type ^1H-^{15}N-NOE spectra were recorded using a 500 μM sample in a 500 MHz spectrometer (20); the titrations were performed with a water flip-back-embedded gradient enhanced [^1H,^{15}N]-HSQC pulse sequence (21) on a ^1H 600 MHz instrument. Lyophilized aliquots of migfilin peptides (0.25-, 0.5-, 1-, 2-, 4-, 6-, 8-, and 12-fold excess over 100 μM protein) were titrated into the protein samples. Where appropriate, the ligand-to-protein ratios were corrected for dilution by weighing the NMR sample tube. The NMR data were processed and analyzed using NMRPipe (22) and SPARKY (www.cgl.ucsf.edu/home/sparky). To map the binding site the combined induced chemical shifts (the chemical shift change upon ligand binding) of amide N-H [$\Delta\delta_{(HN,N)}$] were derived using,

$$\Delta\delta_{(HN,N)} = \sqrt{(\Delta\delta_{HN})^2 + (0.154 \times \Delta\delta_N)^2} \qquad \text{(Eq. 1)}$$

where $\Delta\delta_{HN}$ and $\Delta\delta_{HN}$ are the ligand-induced chemical shift

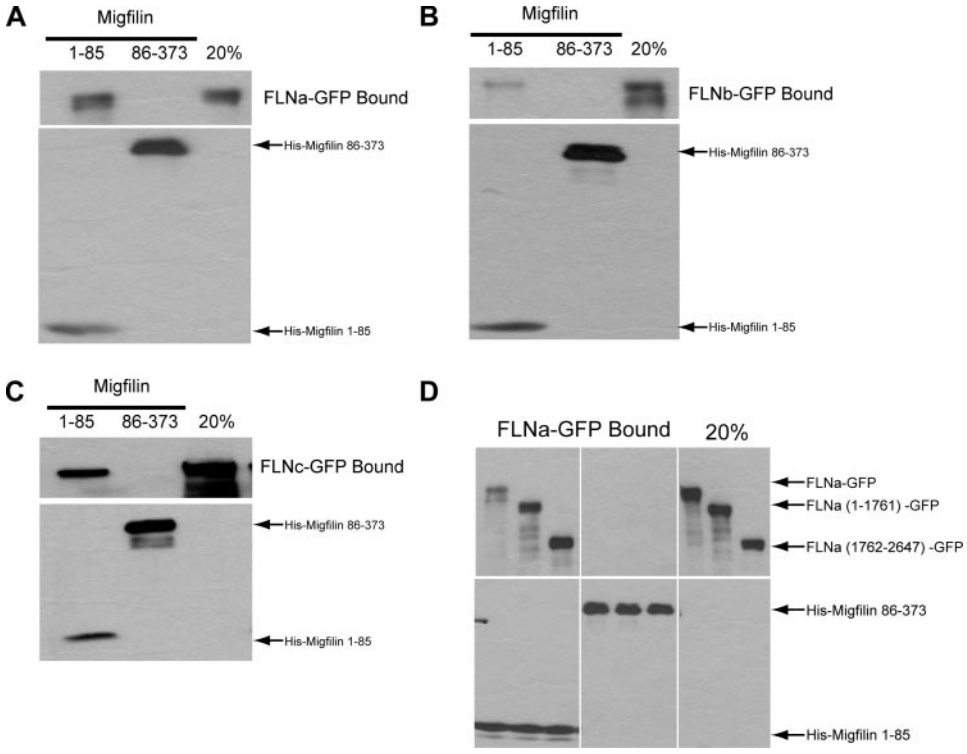

FIGURE 1. **The N-terminal 85 amino acids of migfilin bind to filamins A, B, and C.** *A–D*, pull-down assays were performed using lysates of Chinese hamster ovary cells transfected with (*A*) FLNa-GFP, (*B*) FLNb-GFP, (*C*) FLNc-GFP, or (*D*) FLNa-GFP fragments, FLNa-(1–1761) (ABD + rod 1) or FLNa-(1762–2647) (rod 2) to beads coated with migfilin-(1–85) or –(86–373). Bound proteins were detected by immunoblotting with anti-GFP antibodies and loading with anti-His antibodies. 20% lanes represent corresponding percentage of the starting material in the binding assay.

deviations produced in the proton and nitrogen dimensions, respectively (23). The three-dimensional mapping model, using an optical spectrum color gradient to represent the magnitude of the induced chemical, was generated with MOLMOL (24).

The binding constants were fitted, assuming a 1:1 interaction model, to typical fast-exchange tracks of peaks with the largest shifts in the proton and nitrogen dimensions as follows,

$$\frac{\Delta\delta}{\Delta\delta_{max}} = \frac{[P]_0 + [L]_0 + K_d - \sqrt{([P]_0 + [L]_0 + K_d)^2 - 4[P]_0[L]_0}}{2[P]_0} \quad \text{(Eq. 2)}$$

where $\Delta\delta_{max}$ stands for the maximum shift observed at saturating ligand concentration; $[P]_0$ and $[L]_0$ are the total protein and ligand concentration; in practice, $[L]_0$ was replaced by the product of protein concentration and the ligand-to-protein ratio. Two-parameter fitting (*i.e.* K_d and $\Delta\delta_{max}$) was realized using Origin software.

Crystallization and Data Collection—Recombinant IgFLNa21 was produced and purified as previously described (15). Crystals were produced at 22 °C by hanging drop vapor diffusion using an equimolar (1 mM) mixture of IgFLNa21 and migfilin Pro^5–Pro^{19} peptide. Final crystals were grown in 1.7 M $(NH_4)_2SO_4$, 5% 2-propanol with the use of seeding. Crystals were transferred into 25% glycerol, 1.6 M $(NH_4)_2SO_4$, 5% 2-propanol and frozen in liquid N_2. The diffraction data were collected at 100 K at the European Synchrotron Radiation Facility beamline ID14-2.

Structure Determination and Refinement—The data were processed with XDS (Max Planck Institute for Medical Research, Heidelberg, Germany) (25) and the structure was solved by molecular replacement with the program Phaser (26) using Protein Data Bank (PDB) entry 2BRQ chain A as the search model. Refinement and model building were performed by programs Arp/Warp (27), Refmac5 (28), and Coot (29). The Pro^5–Pro^{19} migfilin peptide was built by hand with Coot. Medium tight non-crystallographic symmetry restrains between chains A and B were used in the refinement. The structure factors and coordinates of the structure have been deposited as PDB entry 2W0P. The data collection and structure refinement statistics are summarized in Table 1. Crystallographic figures were generated and root mean square deviations of superimposed structures were calculated by PyMol (DeLano Scientific, San Carlos, CA). The interaction surfaces were analyzed with the PROTORP server (www.bioinformatics.sussex.ac.uk/protorp/index.html).

RESULTS

The N-terminal 85 Amino Acids of Migfilin Bind to Filamin A, B, and C—Migfilin, or its alternatively spliced variants, have been described as filamin-binding proteins (3, 4) and the N-terminal portion of migfilin has been implicated in filamin binding. To test the generality of this interaction we produced two recombinant migfilin fragments spanning the complete molecule; an N-terminal fragment (migfilin-(1–85)) and a larger 86–373 fragment encompassing the central region and the 3 C-terminal LIM domains. These fragments were expressed in bacteria as N-terminal His-tagged proteins and purified on His-bind resin. Using migfilin-coated beads in pull-down assays we confirmed that migfilin-(1–85) binds FLNa-GFP from Chinese hamster ovary cell lysates, whereas the C-terminal 86–373 portion displayed no detectable FLNa binding (Fig. 1*A*). Similar results were obtained for FLNb-GFP (Fig. 1*B*) and FLNc-GFP (Fig. 1*C*).

Migfilin Binds Sites in Both Rod 1 and 2 of FLNa—Migfilin has been shown to bind sites in the rod 2 region (IgFLN16–24) of FLNa and FLNc (3), whereas the migfilin splice variant FBLP-1, which contains the filamin-binding 1–85 portion, was reported to bind to IgFLNb10–13, within FLNb rod 1 (4). We assessed the ability of His-tagged migfilin fragments to pull-down FLNa amino acids 1–1761-GFP (ABD + rod 1), which contains the actin-binding domains and FLNa amino acids 1762–2647-GFP (rod 2). As shown in Fig. 1*D* the N terminus of

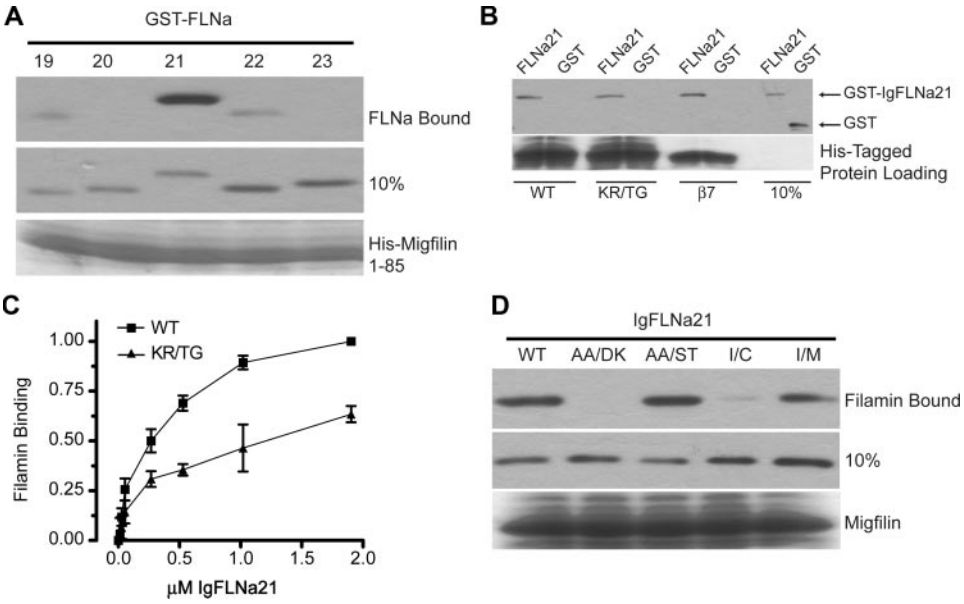

FIGURE 2. **Migfilin binds IgFLNa21 directly.** *A* and *B*, direct pull-down assays were performed using (*A*) purified GST-IgFLNa19, -20, -21, -22, or -23 to migfilin-(1–85)-coated beads or (*B*) purified GST-IgFLNa21 or GST to migfilin-(1–85), migfilin K7T/R8G 1–85 or integrin β7-coated beads. Bound proteins were detected by immunoblotting with anti-GST antibodies. *C*, protein binding was quantified by densitometry and expressed as filamin binding (arbitrary units) was calculated as the ratio of filamin bound to filamin in the loading control, normalized to maximal filamin binding in each experiment (mean ± S.E.; $n \geq 3$). *D*, pull-down assays were performed using purified (*D*) GST-IgFLNa21 containing mutations in strands C (A2272D,A2274K or A2272S,A2274T) or D (I2283C or I2283M) to migfilin-(1–85)-coated beads. 10% lanes represent the corresponding percentage of the starting material in the binding assay.

migfilin bound both FLNa fragments, whereas the C-terminal portion failed to interact with either FLNa fragment. Thus the N-terminal 85 amino acids of migfilin mediate binding to all 3 filamins and migfilin can bind filamin at sites in 1–1761 and 1762–2647.

Migfilin Binds IgFLNa21 Directly—Although we have demonstrated that migfilin binds to both rod 1 and 2 of FLNa in pull-down assays, most FLN-interacting proteins interact with sites in rod 2 (8, 13, 14). We have also proposed that the CD face of IgFLNa domains in this region serves as a general ligand binding interface (15). We therefore sought to further characterize the interactions between migfilin and IgFLNa domains in rod 2. Using yeast two-hybrid assays, Tu *et al.* (3) localized the migfilin binding site to IgFLNc21 in the rod 2 fragment of FLNc and mapped the binding site in FLNa to IgFLNa domains 19–24. We used direct binding assays with individual GST-IgFLNa domains and His-tagged migfilin-(1–85) to show that, in a purified system, IgFLNa21 binds migfilin (Fig. 2*A*) but we also detected weak binding to IgFLNa19 and IgFLNa22 (Fig. 2*A*). The interaction between migfilin-(1–85) and IgFLNa21 is specific, as migfilin did not bind to IgFLNa20, IgFLNa23, or to GST (Fig. 2, *A* and *B*). The interaction with IgFLNa21 was dose-dependent and saturable with an apparent K_d of 0.3 ± 0.05 μM (Fig. 2*C*).

We previously characterized the interaction between integrin β subunit cytoplasmic domains and IgFLNa21 and identified point mutations in the C and D strands of the IgFLNa21 β sandwich that inhibited integrin binding (15). To test whether migfilin binds to a similar surface on IgFLNa21, Ala^{2272} and Ala^{2274} in strand C and Ile^{2283} in strand D were mutated in GST-IgFLNa21 and binding to His-migfilin-(1–85) was assessed. Conservative substitutions AA/ST or I/M had little effect on migfilin-IgFLNa21 binding, whereas AA/DK or I/C substitutions strongly inhibited migfilin binding (Fig. 2*D*). This result is very similar to that observed for β7-IgFLNa21 binding, suggesting that migfilin and β7 may bind to a similar site on IgFLNa21.

The Migfilin-(1–85) Is Unstructured When Free in Solution—To further understand the interaction between migfilin and filamin we sought to investigate the molecular structure of the N terminus of migfilin in solution using NMR. The ^{1}H-^{15}N-HSQC spectrum of migfilin-(1–85) (supplemental Fig. S1) has chemical shifts typical of an unstructured species (30). Moreover, heteronuclear ^{1}H-(^{15}N)-NOE experiments showed complete peak inversion for nearly all the N-H cross-peaks, which implies that the protein chain is extremely flexible (31).

Migfilin Residues 5–19 Mediate Binding to FLNa—We previously showed (15, 32) that two isoleucines (Ile^{782} and Ile^{786}) in the bound β7 integrin peptide made important hydrophobic contacts with IgFLNa21. We thus examined the migfilin-(1–85) sequence for candidate filamin-binding sites using a CLUSTAL-W algorithm to align the structurally defined filamin-binding sequences from β7 (15), β2 (33), and IgFLNa20 (16) with migfilin-(1–85). This led to a prediction that residues between Pro^{5} and Pro^{19} could be the filamin-binding site (Fig. 3*A*), consistent with available published data where loss of amino acids 1–24 or the mutation K7T/R8G in migfilin disrupted filamin binding (3). A synthetic, unlabeled 15-mer migfilin Pro^{5}–Pro^{19} peptide was therefore titrated into a U-^{15}N-IgFLNa21 NMR sample. Clear binding was observed with induced peak shifts spread throughout the HSQC spectra of IgFLNa21, confirming binding (Fig. 3*B*). By comparing the ligand ratio-dependent chemical shift perturbations with simulated curves (Fig. 3*C*), the affinity of this interaction is estimated to be ≤1 μM, in agreement with the IgFLNa21-migfilin-(1–85) affinity calculated from pull-down assays (Fig. 2*C*). To examine the interaction of the larger migfilin-(1–85) fragment with IgFLNa21, non-labeled migfilin-(1–85) was titrated into U-^{15}N-IgFLNa21 for NMR studies. Although the long unstructured peptide leads to aggregation at 4-fold excess, the induced shifts were almost identical to those found in the migfilin-(5–19) peptide titration (Fig. 3, *B* and *D*). This experiment strongly suggests that migfilin-(5–19) is the primary filamin binding sequence in intact migfilin. Consistent with our migfilin pull-down assays, an NMR titration with the Pro^{5}–Pro^{19} peptide and U-^{15}N-IgFLNa19 (Fig. 3*E*) revealed binding, but with at least

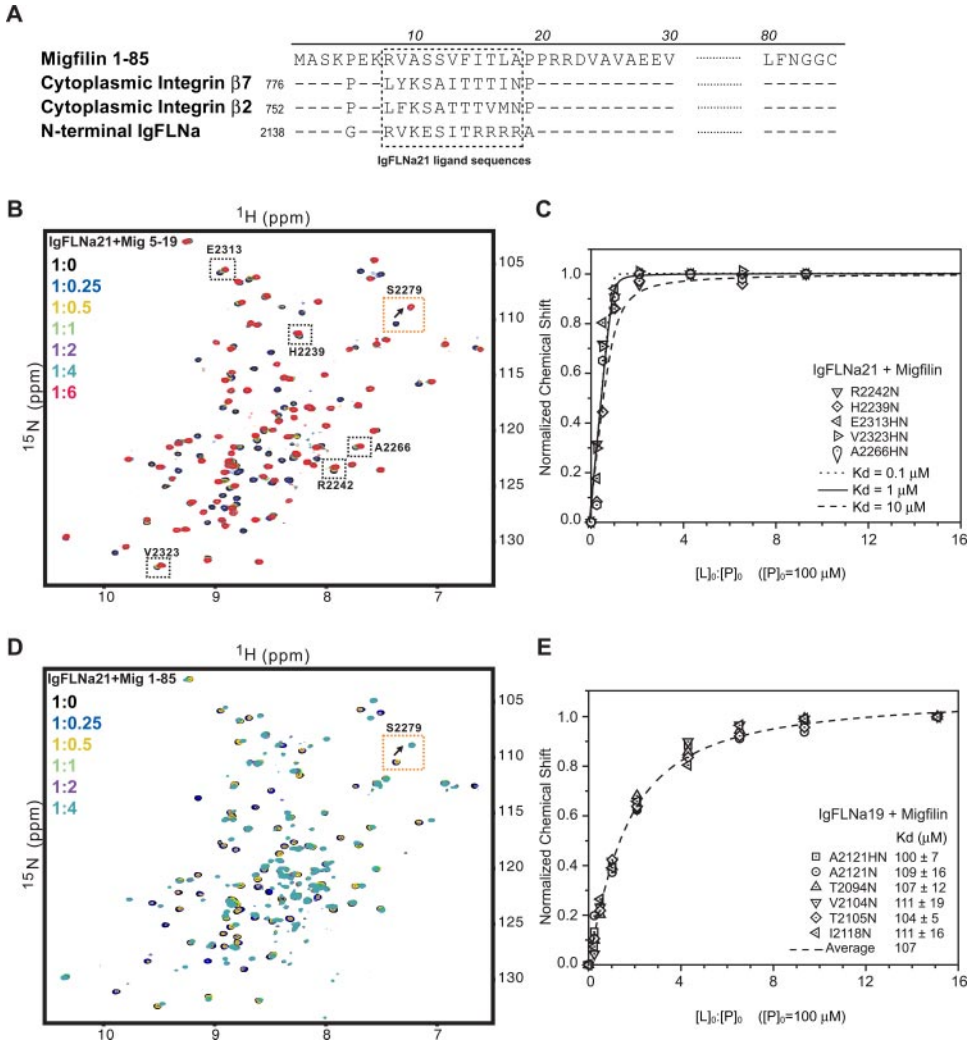

FIGURE 3. **Migfilin residues 5–19 mediate binding to FLNa.** *A*, alignment of the N terminus of migfilin with the IgFLNa21 binding region of β7, β2, and IgFLNa20. *B*, comparison of IgFLNa21 HSQC overlaid spectra showing the effect of addition of the migfilin ^{5}Pro-^{19}Pro-derived peptide; the observed behavior generally corresponds to the slow exchange regime except for a few resonances with small shifts, outlined in *black boxes*. The color scheme of the overlaid spectral layers is indicated. *C*, normalized induced chemical shifts of those resonances with typical fast exchange behavior were plotted against the ligand-to-protein ratio for IgFLNa21. Due to the relatively large error for those small shifts and the relatively high affinity, the data fitting was not very successful. Comparison with the theoretical simulated binding curves for K_d at 0.1, 1, and 10 μM, the affinity for migfilin binding to IgFLNa21 is estimated to be ≤1 μM. *D*, overlaid HSQC spectra of IgFLNa21 upon titration by migfilin-(1–85); the corresponding induced shifts are nearly identical to the above short migfilin peptide (*C*), although some peaks are broadened, probably due to aggregation. *E*, migfilin added to IgFLNa19 gives many more fast exchange peaks, and, in that case, the induced chemical shifts could be readily fitted to a K_d of about 107 μM.

a 100-fold lower affinity than IgFLNa21, suggesting that residues 5–19 of migfilin are relatively specific for IgFLNa21.

Migfilin Binds to the CD-face of IgFLNa21 in a Manner Similar to Integrin β Tails—To study the interaction of IgFLNa21 and migfilin at the atomic level we co-crystallized the migfilin Pro^{5}–Pro^{19} peptide with IgFLNa21. The crystals belonged to the space group $P2_12_12_1$ and data up to 1.9-Å resolution was used. The structure was solved by molecular replacement using the structure of IgFLNa21 (PDB entry 2BRQ chain A)(15) as the search model. The molecular replacement gave a single solution with two IgFLNa21 molecules in the asymmetric unit (R_{work} = 32.2%, R_{free} = 37.4%). Electron density for residues 8–16 of the migfilin peptide was clearly observable between the two IgFLNa21 molecules. The structure was refined to R_{work} = 20.9% and R_{free} = 23.9% (Table 1). In the final model the two IgFLNa21 molecules were nearly identical to each other (root mean square deviation 0.245 Å for 353 atoms) and to the previously solved IgFLNa21 structures (root mean square deviation 0.388 Å for 345 atoms when compared with PDB entry 2BRQ). The single migfilin peptide is hydrogen bonded to β strand C of both IgFLNa21 molecules and thus connects the two CFG β sheets together (Fig. 4, *A–C*). In this kind of arrangement the peptide cannot have identical interactions with both IgFLNa21 molecules. The accessible surface area covered by the peptide is 501 Å^2 on IgFLNa chain A and 425 Å^2 on chain B. Both of the migfilin peptide interactions observed are very similar to those between integrin β2 and β7 cytoplasmic domains and IgFLNa21 (15, 33) (Fig. 4, *D–G*). In addition to the main chain hydrogen bonding, the main interactions between the peptide and IgFLNa chain A were mediated by possible hydrogen bonding of Ser^{11} and hydrophopic side chain contacts of Val^{13} and Ile^{15} (Fig. 4*D*). The corresponding interactions with IgFLNa21 chain B were mediated by Ser^{12}, Phe^{14}, and Thr^{16} (Fig. 4*E*).

To investigate the nature of the interaction between migfilin and IgFLNa21 in solution, the shifts induced in residues of U-^{15}N-IgFLNa21 by the migfilin ^{5}P-^{19}P peptide were analyzed by NMR and mapped on the crystal structure of IgFLNa21 (Fig. 5*A*). The chemical shifts induced in IgFLNa21 are concentrated on the CD face of IgFLNa21 (Fig. 5*B*) and are similar to that observed for the titration of β7 peptide to IgFLNa21 (15). Together with the data from x-ray crystallography (Fig. 4) and pull-down assays that show that mutagenesis of the C or D strands inhibits migfilin binding (Fig. 2*D*), this clearly indicates migfilin binding to the CD face of IgFLN domains.

The crystallographic data indicate that, under the conditions used for crystal growth, a single migfilin peptide can bind two IgFLNa21 domains. In both modes the interaction is similar to previously characterized integrin-IgFLNa21 interactions (15, 33) (Fig. 4, *F* and *G*). There was no evidence for the formation of stable oligomers in our solution state NMR experiments. This suggests that only one of the two interactions modes seen in the crystal may be relevant. To

TABLE 1
Crystallographic data collection statistics

Data collection	
Beamline	ESRF ID14-2
Wavelength, Å	0.933
Space group	$P2_12_12_1$
Cell dimensions	
a, *b*, *c*, Å	36.89, 68.48, 85.22
α, β, γ (degree)	90, 90, 90
Resolution range, Å	32.48–1.90 (1.95–1.90)[a]
R_{sym}, %	13.4 (74.1)
$I/\sigma I$	13.5 (2.35)
Completeness, %	99.9 (97.7)
Redundancy	2.54 (2.50)
Refinement	
Resolution range, Å	32.48–1.90 (1.95–1.90)
No. of reflections	
Refinement	16,730 (1208)
Test set	895 (68)
R_{work}/R_{free}, %	20.9/23.9 (23.3/28.5)
Correlation coefficients $F_o - F_c/F_o - F_c$ free	0.943/0.926
No. of atoms	1,532
Protein	1,452
Heterogen	10
Solvent	70
Root mean square differences	
Bond lengths, Å	0.021
Bond angles (degree)	1.789
Average *B*-factor, Å^2	24.88
Protein	24.24
Peptide	23.36
Solvent	29.62
B-factor from Wilson plot	23.68
Amino acids in Ramachandran diagram (%)	
In most favored regions	94.7
In additional allowed regions	5.3
In generously allowed regions	0.0

[a] Values of the last resolution shell in parentheses.

investigate this, we tested the binding of a series of migfilin mutants.

The IgFLNa21 chain A interaction involves migfilin residues Ser^{11}, Val^{13}, and Ile^{15} (Fig. 4*D*), whereas chain B interaction involves migfilin residues Ser^{12}, Phe^{14}, and Thr^{16} we therefore mutated some of these residues in the migfilin-(5–19) peptide and assessed binding to IgFLNa21 by NMR. Peptides containing glutamate substitutions in place of Ser^{11} or Ile^{15} were observed to exhibit either typical fast (S11E) or intermediate (I15E) exchange behavior (an example of the observed behavior for a IgFLNa21 peak on addition of WT, S11E, and I15E mutant migfilin peptides is shown in Fig. 5*C*); the binding affinity in this case was at least 50-fold less than wild-type migfilin (Fig. 5*E*). In contrast, the two adjacent residues, Ser^{12} and Phe^{14}, produced insignificant inhibition when changed to glutamate (Fig. 5*D*). This strongly suggests that the IgFLNa21 chain A-migfilin interaction represents the primary binding pattern in solution.

To further test the role of Ser^{11} and Ile^{15} for the migfilin-filamin interaction Ser^{11} was mutated to Asp and Ile^{15} to Glu and the ability of His-tagged migfilin-(1–85) or migfilin mutants to bind GST-IgFLNa21 was assessed. Both the S11D and I15E mutations blocked IgFLNa21 binding (Fig. 5*E*). Thus, Ser^{11} and Ile^{15} are important for the binding of migfilin-(1–85) to IgFLNa21, consistent with the interaction seen between chain A and the migfilin peptide in our crystal structure.

Tu *et al.* (3) previously reported that a K7T/R8G mutation in GFP-migfilin disrupted its interaction with filamin. These residues lie at the N-terminal edge of the filamin-binding peptide (Lys^7 is not visible in our crystal structure, whereas Arg^8 is the first migfilin residue in the interface). We therefore tested the effect of this double mutation on direct migfilin-filamin interactions. Although a fixed dose binding assay of 1 μg of purified GST-IgFLNa21 to migfilin-(1–85) KR/TG failed to show any clear inhibition in binding (Fig. 2*B*), a more extensive dose-response analysis showed that migfilin KR/TG does indeed reduce migfilin-filamin binding somewhat (Fig. 2*C*).

Our experiments, with purified migfilin-derived peptides and isolated filamin domains thus indicate that migfilin binds to the CD face of IgFLNa21 and IgFLNa19 in a similar way to the known β7 integrin-FLNa21 interaction. As shown in Fig. 1*D*, migfilin also binds to sites in FLNa–(1–1761). We therefore tested whether S11D or I15E mutations in migfilin, which inhibit binding to IgFLNa21, could impact migfilin binding to intact FLNa. As shown in Fig. 5*F*, these mutations strongly inhibited the ability of migfilin-(1–85) to pull-down FLNa-GFP from cell lysates. Furthermore, migfilin-(1–85) I15E was unable to bind either FLNa-(1–1761) (ABD + rod 1) or FLNa-(1762–2647) (rod 2) of FLNa (Fig. 5*G*). This suggests that migfilin may interact with a variety of IgFLN domains via a similar mechanism.

Migfilin Competes with Integrin β Tails for Binding to IgFLNa21—Our data indicate that both migfilin and β integrins bind to the CD face of IgFLNa21 (15). To test if migfilin can compete with β integrins for IgFLNa21 binding we examined the effect of increasing amounts of a migfilin-(5–19) peptide on the binding of GST-IgFLNa21 to limiting quantities of integrin β7 tails. The migfilin peptide caused a dose-dependent inhibition of IgFLNa21 binding to β7 integrin tails (Fig. 6). The inhibition with a control migfilin peptide was reduced in comparison. Thus unstructured N terminus of migfilin binds to the CD face on IgFLNa21 in a very similar manner to β integrin tails and because it has a higher affinity it can readily compete for filamin binding.

Migfilin-Filamin Interactions Target Migfilin to Stress Fibers—Migfilin has been shown to localize to cell-extracellular matrix focal contacts and to actin stress fibers. It is proposed that adhesion targeting is mediated through binding to kindlin-2, whereas stress fiber localization is mediated via filamin binding (3). We therefore examined the subcellular localization of our migfilin mutants in NIH3T3 cells. Expression of GFP-migfilin resulted in staining of adhesions, with some weak stress fiber staining also evident (Fig. 7*A*). GFP-migfilin-(1–85) showed much stronger actin stress fiber localization and, consistent with previous reports (3), failed to localize at focal adhesions (Fig. 7*A*). In spread NIH3T3 cells FLNa is predominantly localized along actin stress fibers (Fig. 7*B*). As expected, GFP-migfilin-(1–85) co-localizes with FLNa in NIH3T3 cells, however, this co-localization in stress fibers is disrupted with filamin-binding defective migfilin mutants. Neither GFP-migfilin-(1–85) S11D nor I15E localize to actin stress fibers but rather display a diffuse staining pattern similar to GFP expressing cells (Fig. 7*B*). In these cells, filamin localization remains at actin stress fibers and is not disrupted by the GFP-migfilin mutants. Cell shape, size, and spreading was not affected in the

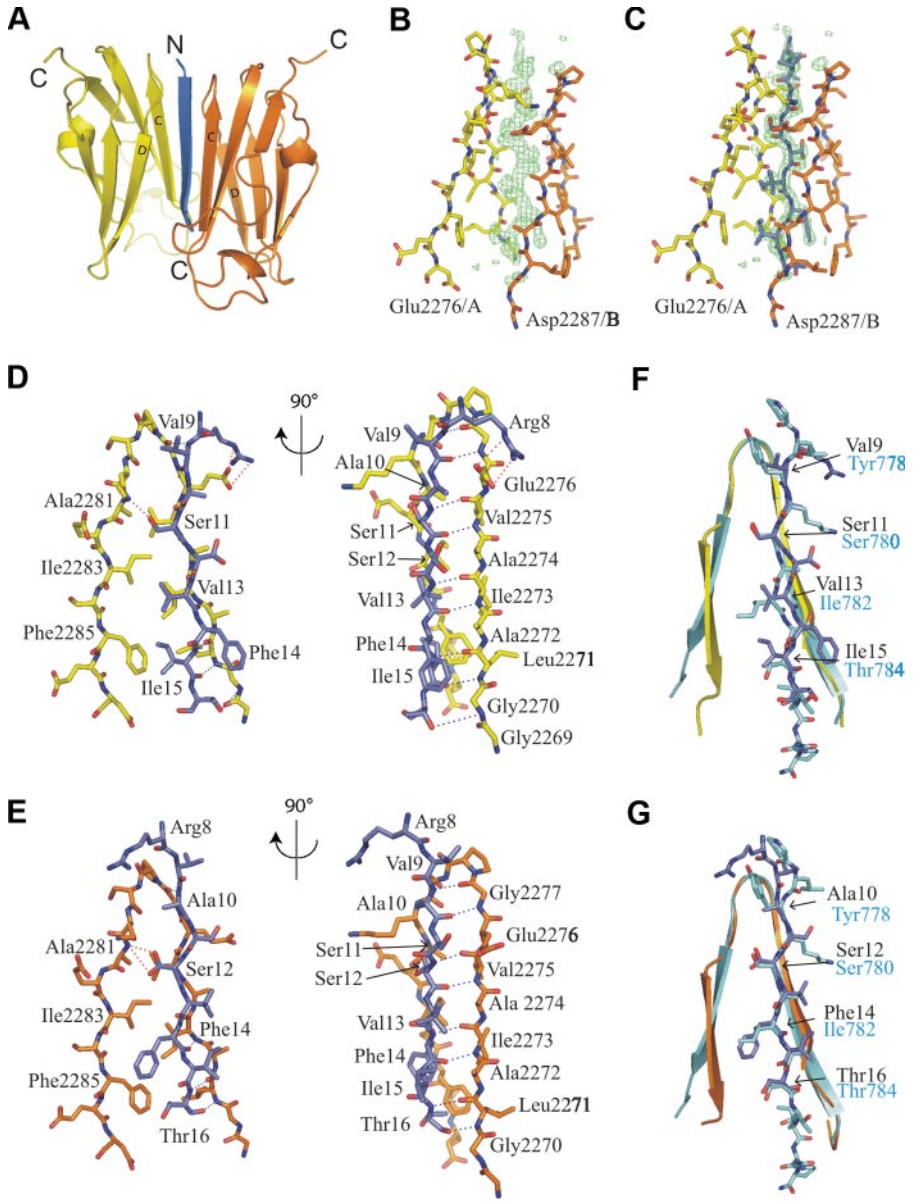

FIGURE 4. **Structure of IgFLNa21/Pro^{5}-Pro^{19} migfilin peptide complex.** *A*, overall structure of the IgFLNa21 Pro^{5}-Pro^{19} migfilin peptide complex shown as a schematic. N and C termini are indicated. Migfilin peptide (*blue*) is surrounded by two IgFLNa21 domains, chain A (*yellow*) and chain B (*orange*). *B*, electron density map ($F_o - F_c$) of the migfilin peptide without peptide calculated from the final model without the peptide and shown at σ level 3.0. *C*, the same panel as *B* but with migfilin peptide. *D*, details of residues participating in the interaction of IgFLNa21 chain A and migfilin peptide. Most side chains of peptide residues interact with residues of the IgFLNa21 D-strand. Residues likely to be important for the interaction are named. The backbone hydrogen bonds are shown with *blue dashed lines* and side chain hydrogen bonds with *red*. Ser^{11} and Val^{13} were modeled in 2 alternative conformations. *E*, details of the side chain interactions between IgFLNa21 chain B and migfilin peptide. *F* and *G*, superposition of the IgFLNa21-β7 integrin complex (PDB 2BRQ) with the IgFLNa21 chain A-migfilin (*F*), or IgFLNa21 chain B-migfilin (*G*) structures. IgFLNa21 strands C and D are shown as schematics with the integrin and migfilin peptides as *stick models*. Colors of the IgFLNa21-migfilin complex are as in *panel A*, the IgFLNa21-β7 complex is shown in *pale blue*.

GFP-migfilin expressing cells compared with control GFP expressing NIH3T3 cells (data not shown). Thus filamin binding is required for migfilin localization to actin stress fibers in cells.

DISCUSSION

A link between sites of cell adhesion and the cytoskeleton is essential for regulation of cell shape, motility, and signaling. Migfilin, which localizes at both cell-cell and cell-extracellular matrix adhesion sites, is thought to provide one such link to the actin cytoskeleton through its interaction with the actin-binding and cross-linking protein filamin. Here we have investigated the molecular basis of migfilin interactions with filamin and solved the crystal structure of IgFLNa21 bound to a migfilin peptide. We find that: 1) the N-terminal portion of migfilin, which is present in all 3 splice forms is largely disordered in solution but can bind to FLNa, -b, or -c; 2) the filamin-binding site in migfilin is localized between Arg^{8} and Thr^{16}; 3) there are multiple migfilin-binding sites in FLNa; 4) migfilin binds preferentially to IgFLNa21 and more weakly to IgFLNa19 and -22; 5) migfilin binds to the CD face of IgFLNa21 and mutations in either the C or D strand inhibit this interaction as do mutations at Ser^{11} or Ile^{15} in migfilin; 6) migfilin and integrin β tails bind to a similar site on IgFLNa21 and can compete with one another for binding; and 7) the migfilin-filamin interaction is important for targeting migfilin to stress fibers in cells.

Migfilin had previously been shown to bind sites in rod 2 of FLNa and FLNc and rod 1 of FLNb (3, 4). We confirmed that migfilin can interact with all three filamins and showed binding to both rod 1 and 2 of FLNa. To test whether binding was direct and to map interacting domains we used purified proteins to show that migfilin bound IgFLNa19, -21, and -22 within the rod 2 region; the strongest binding was observed with IgFLNa21. This suggests that one filamin molecule may directly bind multiple migfilin molecules. The *in vivo* significance of this, and the reason for the enhanced binding to IgFLNa21, remains to be determined; multiple binding sites may, however, permit reinforcement of filamin-mediated links to the actin cytoskeleton or provide redundancy, thus allowing the actin linkage to be maintained in the presence of other filamin-binding proteins.

High-resolution structural data has been reported describing FLNa-integrin (15, 33) and FLNa-GPIbα interac-

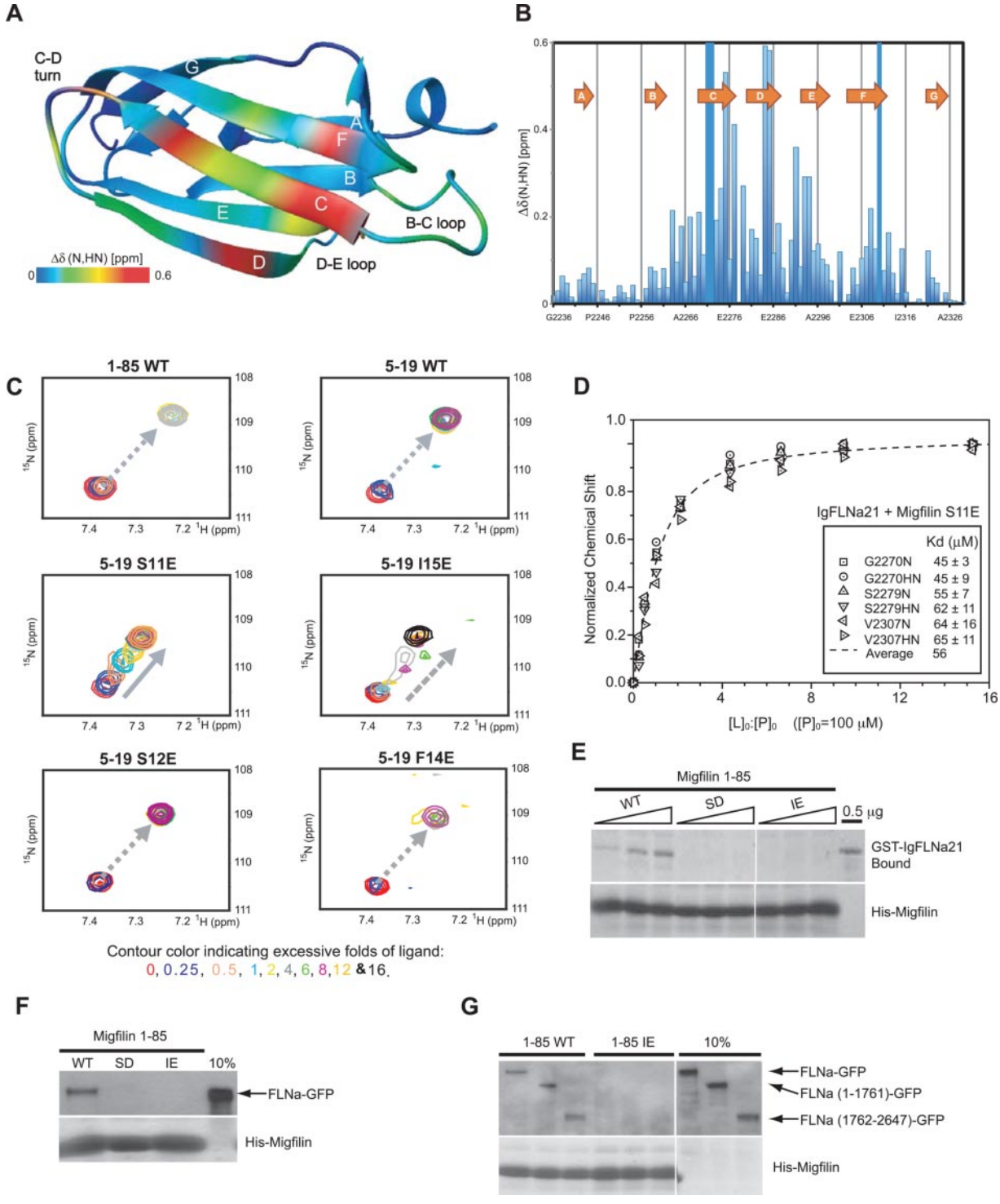

FIGURE 5. **Migfilin binds to the CD face of IgFLNa21 in a manner similar to the integrin β7.** *A*, combined chemical shift perturbations of resonances in the U-^{15}N-IgFLNa21 amide H-Ns induced by a 4-fold excess of migfilin Pro^{5}—Pro^{19}-derived peptide are mapped onto the crystal structure of IgFLNa21 from the IgFLNa21-β7 integrin complex (PDB 2BRQ). Residues are colored according to the size of the shift with the largest shifts shown in *red* and no shifts in *blue*. *B*, chemical shift perturbations are also represented in a two-dimensional bar chart, strongly perturbed but non-assigned residues are denoted by *solid blue bars*. *C*, extracted HSQC spectra of IgFLNa21 residue Ser^{2279} upon addition of migfilin-(1–85)/5–19 WT or S11E, S12E, F14E, and I15E peptides. The color scheme of the overlaid spectra is shown in the figure. (When the binding is tight the peaks are in slow exchange with one peak decreasing and the other increasing on addition of ligand. With weaker binding (S11E and I15E) the peaks are in fast exchange and migrate from one position to another.) *D*, normalized induced chemical shifts of resonances with typical fast exchange behavior and relatively large shifts were plotted against the ligand-to-protein ratio for IgFLNa21 binding to migfilin S11E with a theoretically simulated binding curve shown as a *dashed line*. *E*, direct pull-down assays were performed using GST-IgFLNa21 to migfilin-(1–85) WT, S11D, or I15E. *F*, pull-down assays were performed using lysates of Chinese hamster ovary cells transfected with FLNa-GFP to beads coated with migfilin-(1–85) wild type, S11D, or I15E. *G*, binding of FLNa, FLNa-(1–1761) (ABD + rod 1), or FLNa-(1762–2647) (rod 2) to beads coated with migfilin-(1–85) wild type or I15E. 10% lanes represent corresponding percentage of the starting material in the binding assay.

tions (34), IgFLNc dimerization (11), and an autoinhibitory IgFLNa20-IgFLNa21 interaction (16). In all cases ligand binding occurs at the CD face of the IgFLN domain with the binding partner forming a new β strand anti-parallel to strand C, which extends the CFG sheet of the IgFLN domain. The data reported here provide further support for the idea that the CD face is a general ligand binding surface on IgFLN (15). Crystallography reveals that migfilin peptides bind the CD face of IgFLNa21 in a manner very similar to integrin β tail peptides. Two modes of binding are observed in the crystal state (chain A and chain B bind one migfilin strand). Both interaction modes are similar to previously characterized IgFLN-ligand interactions but NMR and mutagenic analyses suggest that the dominant interaction in solution is the one represented by chain A (Figs. 4 and 5). The interface in this case buries a slightly larger surface than the B chain interaction. The structure-based sequence alignment of the chain A mode is as shown in Fig. 3*A*. We do not exclude that under certain contexts migfilin may employ both binding modes to engage two IgFLNs, either from the same or different FLN molecules.

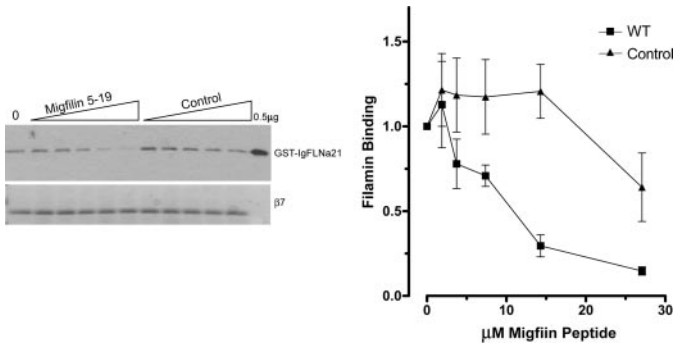

FIGURE 6. **Migfilin competes with integrin β tails for binding to IgFLNa21.** Direct pull-down assays were performed using purified GST-IgFLNa21 to β7 tails in the presence of migfilin-(5–19) or control peptide. Protein binding quantified by densitometry and expressed as filamin binding (arbitrary units) was calculated as the ratio of filamin bound to filamin bound in the absence of peptide in each experiment (mean ± S.E.; $n \geq 3$). Bound proteins were detected by immunoblotting with anti-GST antibodies. 10% lanes represent the corresponding percentage of the starting material in the binding assay.

It is clear that migfilin residues 8–16 encompass the major determinant for migfilin binding to filamins and that the CD face of IgFLNa19 and IgFLNa21 provide the interface. Although it remains possible that other regions also contribute to the interaction *in vivo*, mutations in either the C or D strand of the IgFLNa domain can inhibit migfilin binding as do mutations at Ser^{11} or Ile^{15} in migfilin. Ser^{11} or Ile^{15} mutations also inhibit the interaction of migfilin with full-length filamins suggesting some conservation between all migfilin-IgFLN domain interactions. Thus, CD face residues are good initial targets for mutagenesis in future attempts to identify mutations that can inhibit the association of other filamin-binding proteins.

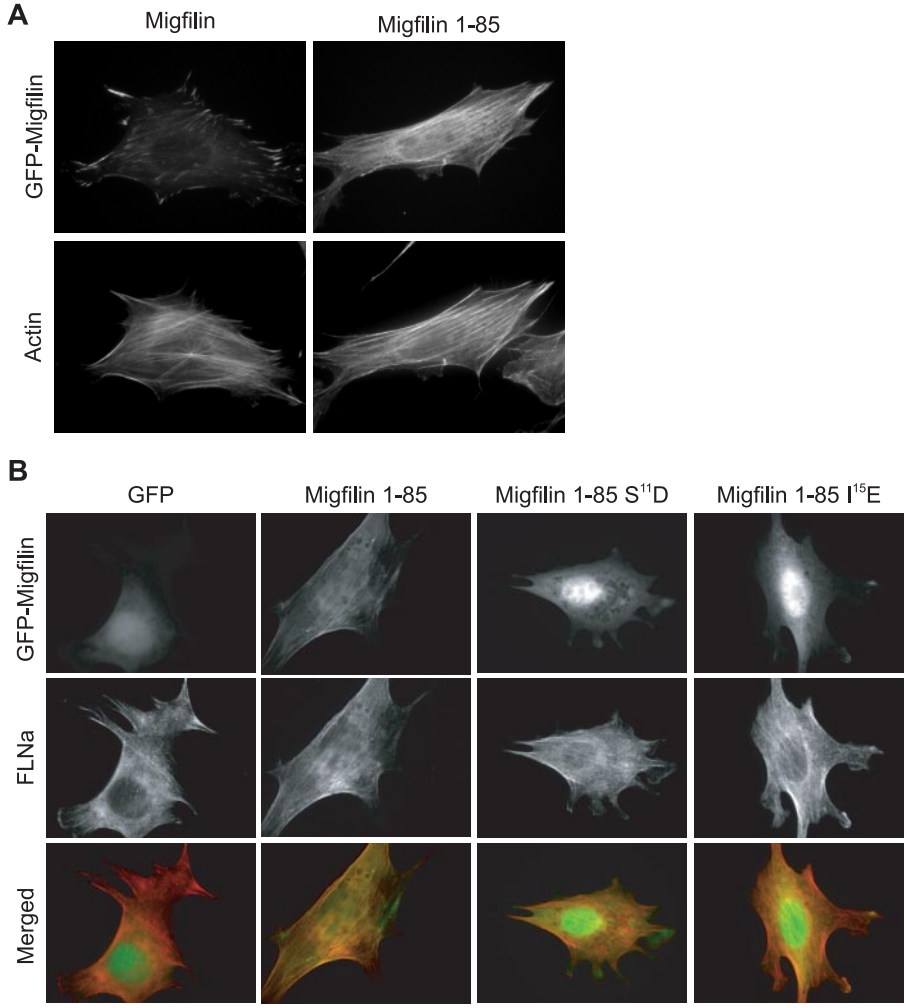

FIGURE 7. **Migfilin-filamin interactions target migfilin to stress fibers.** Immunofluorescence of GFP-migfilin or 1–85 mutant-transfected NIH3T3 cells attached to fibronectin-coated coverslips for 4 h prior to fixation. *A*, cells were stained for actin with phalloidin-Alexa 568; or *B*, endogenous FLNa.

The ability of the CD face of IgFLN domains to bind various filamin ligands suggests that competition may be a regulatory mechanism. We tested this hypothesis by assessing the impact of the filamin-binding migfilin peptide on integrin binding to IgFLNa21. As predicted, the filamin-binding peptide, but not a scrambled peptide control, inhibited filamin binding to integrin β tails. Competition between the many different filamin binding partners may thus provide a mechanism to regulate filamin interactions and downstream signaling. In the case of integrin-filamin interactions, this may provide a mechanism for switching between different links to the actin cytoskeleton, mediated either directly via integrin-FLN interactions or potentially through, integrin-kindlin-migfilin-FLN complexes (3, 35–37).

Our finding that phospho-mimicking S11E or S11D mutations inhibited migfilin binding to filamin suggests phosphorylation as another potential mechanism for regulating migfilin-filamin interactions. It is not known whether migfilin is phosphorylated *in vivo* but the sequence surrounding Ser^{11} is consistent with phosphorylation at that site by basophilic serine/threonine kinases such as those in the AGC or CAM kinase families.[7] If this site is indeed a kinase substrate, based on the effect of phospho-mimicking mutations, we predict that phosphorylation would inhibit migfilin binding to filamin. We note that there is specificity in this interaction as phospho-mimicking mutations at the adjacent Ser^{12} residue did not inhibit binding when assessed by NMR spectroscopy.

The binding of migfilin to all three filamins, the number of migfilin-binding IgFLN domains (at least 4 in FLNa), and our observation that filamin mutations that prevent migfilin binding also prevent binding of other filamin ligands makes it difficult to investigate the functional significance of migfilin-filamin interactions using filamin mutants or filamin-deficient cells. However, identification and characterization of migfilin mutants defective in filamin binding indicates that filamin binding is required for targeting to actin stress fibers in stably adherent spread cells. It will be important to determine the downstream functional consequences of this interaction in rescue experiments when migfilin knock-out animals or cells become available.

In summary we have used structural and biochemical analyses to investigate the interaction between filamin and migfilin, a recently identified protein implicated in regulation of cell motility, cell shape, and gene transcription (5). Our results reveal multiple binding sites in filamins and show that migfilin uses a conserved ligand-binding surface on IgFLN domains. Consequently migfilin can compete with other filamin ligands. This has consequences for our understanding of the assembly and remodeling of filamin signaling complexes and may provide a means for switching integrins links to the cytoskeleton.

Acknowledgments—We acknowledge the European Synchrotron Radiation Facility for provision of synchrotron radiation and thank Dr. Carlo Petosa for assistance in using beamline ID14-2 and Dr. Titus Boggon for helpful discussions.

REFERENCES

1. Evans, E. A., and Calderwood, D. A. (2007) *Science* **316,** 1148–1153
2. Zaidel-Bar, R., Itzkovitz, S., Ma'ayan, A., Iyengar, R., and Geiger, B. (2007) *Nat. Cell Biol.* **9,** 858–867
3. Tu, Y., Wu, S., Shi, X., Chen, K., and Wu, C. (2003) *Cell* **113,** 37–47
4. Takafuta, T., Saeki, M., Fujimoto, T. T., Fujimura, K., and Shapiro, S. S. (2003) *J. Biol. Chem.* **278,** 12175–12181
5. Wu, C. (2005) *J. Cell Sci.* **118,** 659–664
6. Papachristou, D. J., Gkretsi, V., Tu, Y., Shi, X., Chen, K., Larjava, H., Rao, U. N., and Wu, C. (2007) *Histopathology* **51,** 409–508
7. Zhang, Y., Tu, Y., Gkretsi, V., and Wu, C. (2006) *J. Biol. Chem.* **281,** 12397–12407
8. Stossel, T. P., Condeelis, J., Cooley, L., Hartwig, J. H., Noegel, A., Schleicher, M., and Shapiro, S. S. (2001) *Nat. Rev. Mol. Cell. Biol.* **2,** 138–145
9. van der Flier, A., and Sonnenberg, A. (2001) *Biochim. Biophys. Acta* **1538,** 99–117
10. Gorlin, J. B., Yamin, R., Egan, S., Stewart, M., Stossel, T. P., Kwiatkowski, D. J., and Hartwig, J. H. (1990) *J. Cell Biol.* **111,** 1089–1105
11. Pudas, R., Kiema, T. R., Butler, P. J., Stewart, M., and Ylanne, J. (2005) *Structure* (*Camb.*) **13,** 111–119
12. Nakamura, F., Osborn, T. M., Hartemink, C. A., Hartwig, J. H., and Stossel, T. P. (2007) *J. Cell Biol.* **179,** 1011–1025
13. Feng, Y., and Walsh, C. A. (2004) *Nat. Cell Biol.* **6,** 1034–1038
14. Popowicz, G. M., Schleicher, M., Noegel, A. A., and Holak, T. A. (2006) *Trends Biochem. Sci.* **31,** 411–419
15. Kiema, T., Lad, Y., Jiang, P., Oxley, C., Baldassarre, M., Wegener, K. L., Campbell, I. D., Ylanne, J., and Calderwood, D. A. (2006) *Mol. Cell* **21,** 337–347
16. Lad, Y., Kiema, T., Jiang, P., Pentikainen, O. T., Coles, C. H., Campbell, I. D., Calderwood, D. A., and Ylanne, J. (2007) *EMBO J.* **26,** 3993–4004
17. van der Flier, A., Kuikman, I., Kramer, D., Geerts, D., Kreft, M., Takafuta, T., Shapiro, S. S., and Sonnenberg, A. (2002) *J. Cell Biol.* **156,** 361–376
18. Lad, Y., Harburger, D. S., and Calderwood, D. A. (2007) *Methods Enzymol.* **426,** 69–84
19. Baldassarre, M., Pompeo, A., Beznoussenko, G., Castaldi, C., Cortellino, S., McNiven, M. A., Luini, A., and Buccione, R. (2003) *Mol. Biol. Cell* **14,** 1074–1084
20. Farrow, N. A., Muhandiram, R., Singer, A. U., Pascal, S. M., Kay, C. M., Gish, G., Shoelson, S. E., Pawson, T., Forman-Kay, J. D., and Kay, L. E. (1994) *Biochemistry* **33,** 5984–6003
21. Schleucher, J., Schwendinger, M., Sattler, M., Schmidt, P., Schedletzky, O., Glaser, S. J., Sorensen, O. W., and Griesinger, C. (1994) *J. Biomol. NMR* **4,** 301–306
22. Delaglio, F., Grzesiek, S., Vuister, G. W., Zhu, G., Pfeifer, J., and Bax, A. (1995) *J. Biomol. NMR* **6,** 277–293
23. Ayed, A., Mulder, F. A., Yi, G. S., Lu, Y., Kay, L. E., and Arrowsmith, C. H. (2001) *Nat. Struct. Biol.* **8,** 756–760
24. Koradi, R., Billeter, M., and Wuthrich, K. (1996) *J. Mol. Graph.* **14,** 51–55
25. Kabsch, W. (1993) *J. Appl. Crystallogr.* **26,** 795–800
26. Storoni, L. C., McCoy, A. J., and Read, R. J. (2004) *Acta Crystallogr. Sect. D Biol. Crystallogr.* **60,** 432–438
27. Perrakis, A., Morris, R., and Lamzin, V. S. (1999) *Nat. Struct. Biol.* **6,** 458–463
28. Murshudov, G. N., Vagin, A. A., and Dodson, E. J. (1997) *Acta Crystallogr. Sect. D Biol. Crystallogr.* **53,** 240–255
29. Emsley, P., and Cowtan, K. (2004) *Acta Crystallogr. Sect. D Biol. Crystallogr.* **60,** 2126–2132
30. Wishart, D. S., Bigam, C. G., Holm, A., Hodges, R. S., and Sykes, B. D. (1995) *J. Biomol. NMR* **5,** 67–81
31. Kay, L. E., Torchia, D. A., and Bax, A. (1989) *Biochemistry* **28,** 8972–8979
32. Calderwood, D. A., Huttenlocher, A., Kiosses, W. B., Rose, D. M., Woodside, D. G., Schwartz, M. A., and Ginsberg, M. H. (2001) *Nat. Cell Biol.* **3,** 1060–1068
33. Takala, H., Nurminen, E., Nurmi, S. M., Aatonen, M., Strandin, T., Takatalo, M., Kiema, T., Gahmberg, C. G., Ylanne, J., and Fagerholm, S. C. (2008) *Blood* **112,** 1853–1856
34. Nakamura, F., Pudas, R., Heikkinen, O., Permi, P., Kilpelainen, I., Munday, A. D., Hartwig, J. H., Stossel, T. P., and Ylanne, J. (2006) *Blood* **107,** 1925–1932
35. Stossel, T. P., and Hartwig, J. H. (2003) *Dev. Cell* **4,** 444–445
36. Kloeker, S., Major, M. B., Calderwood, D. A., Ginsberg, M. H., Jones, D. A., and Beckerle, M. C. (2003) *J. Biol. Chem.* **279,** 6824–6833
37. Shi, X., Ma, Y. Q., Tu, Y., Chen, K., Wu, S., Fukuda, K., Qin, J., Plow, E. F., and Wu, C. (2007) *J. Biol. Chem.* **282,** 20455–20466

[7] B. Turk, personal communication.